2018 IEEE/RSJ International Conference on Intelligent Robots and Systems (IROS)
Madrid, Spain, October 1-5, 2018

Analysis of Dynamic Response of an MRI-Guided Magnetically-Actuated Steerable Catheter System

E. Erdem Tuna, Taoming Liu, Russell C. Jackson, Nate Lombard Poirot, Mac Russell, M. Cenk Çavuşoğlu

***Abstract*— This paper presents a free-space open-loop dynamic response analysis for an MRI-guided magnetically-actuated steerable intra-vascular catheter system. The catheter tip is embedded with a set of current carrying micro-coils. The catheter is directly actuated via the magnetic torques generated on these coils by the magnetic field of the magnetic resonance imaging (MRI) scanner. The relationship between the input current commands and catheter tip deflection angle presents an inherent nonlinearity in the proposed catheter system. The system nonlinearity is analyzed by utilizing a pendulum model. The pendulum model is used to describe the system nonlinearity and to perform an approximate input-output linearization. Then, a black-box system identification approach is performed for frequency response analysis of the linearized dynamics. The optimal estimated model is reduced by observing the modes and considering the Nyquist frequency of the camera system that is used to track the catheter motion. The reduced model is experimentally validated with $3D$ open-loop Cartesian free-space trajectories. This study paves the way for effective and accurate free-space closed-loop control of the robotic catheter with real-time feedback from MRI guidance in subsequent research.**

I. Introduction

Catheter ablation (Fig. 1a) is a widely performed minimally invasive interventional procedure for treatment of atrial fibrillation [1], [2]. In that procedure, the catheter is guided by the physician to the left atrium via passing through the femoral vein, the right atrium and the atrial septal wall. In the left atrium, the tip is steered to reach the desired area, such as the ostia of the pulmonary veins, and radio frequency energy is applied to form barriers to prevent the spread of the irregular electrical signals. For the last decade, robotic catheters have emerged as a promising technology for catheter ablation. So far, two robotic catheter systems received U.S. Food and Drug Administration (FDA) clearances, the Niobe ES mag- netic navigation system [3] (Stereotaxis, St. Louis, MO, USA) for the atrial fibrillation ablation, and the Magellan robotic system [4] (Hansen Medical, Mountain View, CA, USA) for the advanced endovascular procedures. Using a robotic catheter system, the physician can remotely steer the catheter, while seated comfortably in the control room and be safely protected from radiation.

Magnetic resonance imaging (MRI) is a promising imaging method for cardiac ablation procedures due to its superior soft tissue visualization with no radiation exposure [6], [7]. Various MRI-actuated catheters designs were proposed in [8]–[15]. A novel steerable robotic catheter system is proposed by Liu *et al.* in [5], [16]. In the proposed design, the catheter is embedded with a set of current-carrying micro-coils at the tip. It is directly actuated via the magnetic torques generated on these coils by the magnetic field of the magnetic resonance imaging (MRI) scanner. The actuation of the proposed catheter system is not subject to the mechanical transmission problems that exist in other actuation methods (such as tendon-driven [17] and hydraulic [18] actuation), which place the actuators outside the patient body. This magnetic actuation method reduces backlash and friction in the system.

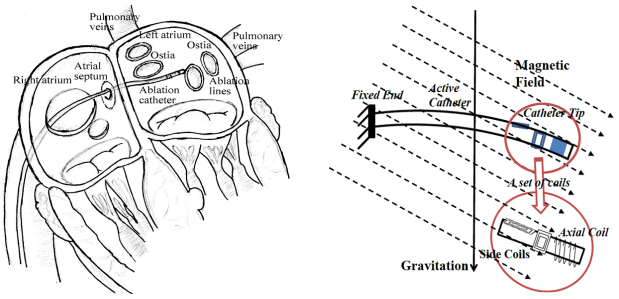

(a) (b)

Fig. 1. (a) Illustration of catheter ablation procedure [5]. (b) Illustration of a proof-of-concept catheter prototype in a magnetic field, including a set of embedded current-carrying coils [5].

In [19], a Jacobian based inverse kinematics method is implemented for the design proposed in [5], [16] using the damped least squares method [20]–[22]. The performance of the proposed inverse kinematics approach is validated using a prototype of the robotic catheter by comparing the actual trajectories of the catheter tip obtained via open-loop control with the desired trajectories. A camera-based vision system is used to track the catheter deflections in the experiments.

As a first step to perform free-space closed loop control, based on the previous work in [5], [16], [19] this paper presents a free-space open-loop dynamic response analysis of the proposed MRI-compatible magnetically actuated steerable catheter system.

For the proposed catheter system, the actuation currents and the deflection angle of the catheter are treated respectively as the overall system input-output. The previous kinematics analysis in [16], exposes a nonlinearity between the input current commands and the output deflection angle. A simple pendulum model is used to model this nonlinearity and to perform an approximate linearization, which yields linearized dynamics between the deflection angle and the net actuation torque obtained from the lineaization step. The

Manuscript received July 15, 2018. This work was supported in part by National Science Foundation under grants CISE IIS-1524363, IIS-1563805, and National Institutes of Health under grant R01 EB018008.

E. E. Tuna, T. Liu, N. L. Poirot, R. C. Jackson, M. Russell, and M. C. Çavuşoğlu are with the Department of Electrical Engineering and Computer Science, Case Western Reserve University, Cleveland, OH 44106, USA (e-mail:eet12@case.edu, txl168@case.edu, rcj33@case.edu, mrr74@case.edu, mcc14@case.edu).

linearized system is then treated as a black-box model and a linear system identification approach is performed to identify the dynamic response analysis of the proposed catheter system, with the net actuation torque and the deflection angle are treated respectively as the system input-output.

In order to model the system nonlinearity effectively with a pendulum, only planar motions are employed when the catheter is aligned with gravity and magnetic field is orthogonal to the gravitational field. Out-of-plane motions are not utilized for model identification as they would further complicate the complex system nonlinearity characterization. Nevertheless, the estimated model is validated with the out-of-plane $3D$ open-loop Cartesian space trajectories. The system response obtained from these experiments are shown to be consistent with the system bandwith calculated from the identification step. This study gives a first insight into frequency characteristics of the proposed catheter system, which together with the previous open-loop control work [19] builds the foundation for accurate free-space closed-loop control of the robotic catheter with real-time feedback from MRI guidance in subsequent research.

The related studies regarding dynamic response analysis of robotic catheters are given in Section II. Dynamic response analysis of the proposed catheter system is described in Section III. The experimental setup and procedures are explained in Section IV-A and the results are presented in Section IV-C. Finally, the discussions and conclusions are given in Section V.

II. Related Studies

Robotic catheters are redundant continuum robots with infinite degrees-of-freedom (DoF) [18]. In [23], Marchese $et\,al.$ presented a high-level system identification algorithm to estimate parameters of a soft spatial fluidic elastomer manipulator. The identification is performed by iteratively adjusting a parameter set p such that a model instantiated from p follows the same N-segment endpoint Cartesian trajectory as measured on the physical system. In [24], Penning $et\,al.$ characterized the frequency response of both the articulation and insertion axes of a continuum manipulator. To evaluate the open loop frequency response of each axis, a chirp position function was input to the system with the catheter in its neutral position. They used Matlab's $tfestimate$ function for the transfer function estimation. Gilbertson et al. [25] presented static and dynamic system identification of a soft actuator system under two different load conditions that loosely mimic actuation in a blood vessel. They used a chirp signal to excite system for dynamic response analysis and performed a grey-box system identification to solve the parameters of nonlinear spring-mass-damper model structure.

In this paper, in order to characterize the catheter system dynamics, a frequency response analysis is performed. When compared to the aforementioned approaches, this study provides a conscise method for the system characterization and instead of trying to model the complex nonlinearites of the system, a linearization approach is followed to simplify the system and then a black-box linear system identification is performed. A chirp current command is used to excite the system to execute planar motions for a certain frequency sweep. Three additional chirp commands with different frequency sweeps are then used for validation of model for $2D$ planar motions. Initially, an approximate input-output linearization is performed using a pendulum model, the remaining approximate linear dynamics are then identified using linear system identification. An auto-regressive model with exogenous input (ARX) is initially selected for the approximate linear system. The resulting model is then simplified by model order reduction and this reduced order model is used for estimating the transfer function of the black-box catheter system. The estimated model is then tested with free-space $3D$ open-loop Cartesian space trajectories on the hardware. An error analysis is performed on the resulting $3D$ trajectories to discuss the validation and frequency characteristics of the estimated model.

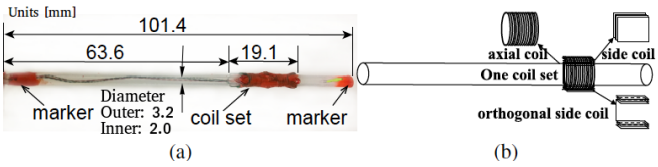

Fig. 2. (a) A proof-of-concept catheter prototype used in the validation experiments. The unit of the dimensions is in mm. (b) Diagram of the catheter prototype with one coil set. Each coil set is composed of two orthogonal side coils and one axial coil.

III. Dynamic Response Analysis

A summary of the catheter actuation and forward kinematics schemes that form the basis of the frequency response analysis presented in this paper are given in Section III-A for completeness. The analysis itself is explained comprehensively in Section III-B.

A. Catheter Actuation Model

In the proposed scheme, the catheter is embedded with one or multiple coil sets along the body. Each coil set includes one axial coil and two orthogonal coils (as shown in Fig. 2 [26]). In a magnetic field, magnetic torques can be generated on these coils by passing through currents. This allows the control of the catheter's three dimensional deflection by controlling the currents. The direction and amplitude of the magnetic torque are determined by the cross product of the magnetic moment from each coil and the magnetic field.

The magnetic torque M_C generated on the electromagnetic coils embedded on the catheter, is given by:

$$M_C = \overrightarrow{\mu_C} \times (R_{C,S} B_{0,S}), \tag{1}$$

where the vector $B_{0,S}$ represents the main (B_0) magnetic field of the MRI system relative to the catheter base frame *S*, $R_{C,S} \in SO(3)$[1] represents the rotation matrix between the coil body frame *C* and the catheter base frame *S*, and $\overrightarrow{\mu_C}$ represents the total magnetization vector of the catheter coils

[1]SO(3) is the rotation group of $\mathbb{R}$ [27]

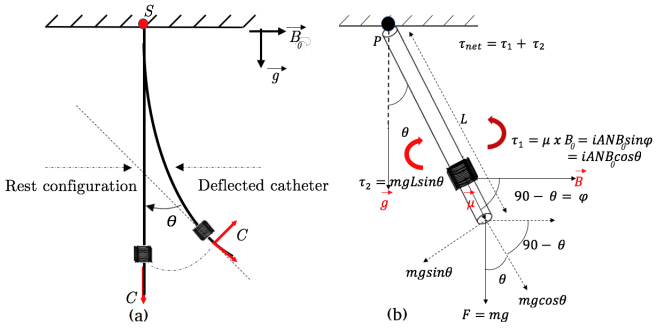

Fig. 3. (a) Experimental configuration of catheter during system identification. $\overrightarrow{B_0}$ denotes the direction B_0 magnetization field vector of the MRI scanner, $\overrightarrow{g}$ denotes the gravity vector direction. S and C are respectively the catheter base and local coil coordinate frames. θ is the deflection angle of the catheter relative to its rest configuration. (b) $2D$ pendulum model of the catheter.

relative to the coil body frame C, which can be expressed as:

$$\overrightarrow{\mu_C} = N_x i_x A_x \overrightarrow{\mu_x} + N_y i_y A_y \overrightarrow{\mu_y} + N_z i_z A_z \overrightarrow{\mu_z}. \quad (2)$$

N_j represents the number of turns in the coil j, A_j is the area enclosed by each turn of the coil j, and i_j is the current through the coil j. For simplicity, it can be transformed to[2]:

$$M_C = -(R_{C,S} B_{0,S})^{\wedge} (Ni), \quad (3)$$

where,

$$N = \begin{bmatrix} N_x A_x & 0 & 0 \\ 0 & N_y A_y & 0 \\ 0 & 0 & N_z A_z \end{bmatrix}, \quad (4)$$

and

$$i = \begin{bmatrix} i_x & i_y & i_z \end{bmatrix}^T. \quad (5)$$

Liu *et al.* [5], [16] developed a method combining a finite differences approach with beam theory and rotation groups to model the proposed MRI-actuated catheter's three dimensional deflection motion, including bending and torsion. In [19], Liu *et al.* presented a Jacobian-based inverse kinematics and open-loop control method for this system. The workspace of the proposed catheter with multiple coil sets is analyzed for optimization of the catheter design by Liu *et al.* [26].

B. System Identification

In system identification, current commands that excite the system by generating the magnetic torques are chosen as the inputs. The deflection angle of the catheter is chosen as the system output (Figs. 3-4).

The cross product in (1) represents an inherent nonlinearity in the system actuation (Fig. 4). In order to approximately perform input-output linearization to simplify system identification, the catheter deflection is modeled by a simple

[2]Symbol $^{\wedge}$ refers to skew-symmetic matrix of the preceding term. By Lie algebra, $so(3)$, of the rotation group $SO(3)$ [27], skew symmetric matrices (3) can be used to represent cross products (1) as matrix multiplications.

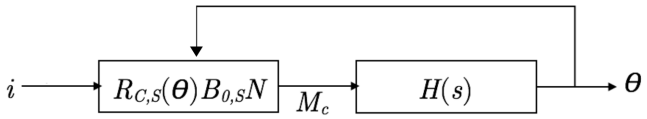

Fig. 4. Input-Output model of the catheter dynamics. i is the input current of the coils and θ is the deflection angle of the catheter. $H(s)$ is the linearized dynamics of the catheter.

planar pendulum with the current carrying coil set at the tip modeled as a solenoid (Fig. 3b). The net actuation torque on the pendulum at pivot point P by the magnetic torque and the gravitational torque is then given by:

$$\begin{aligned} \tau_{net} &= \tau_1 + \tau_2, \\ &= iANB_0 cos\theta - mgLsin\theta. \end{aligned} \quad (6)$$

A is the area of solenoid. N is the number of turns of the solenoid (Fig. 2). L and m are respectively the length and the mass of the catheter prototype. i is the input current commands to the system, $\theta = 90 - \varphi$ is the catheter deflection angle, and φ is the angle between coil tangent (or magnetization vector) and the magnetic field.

In order to perform approximate input-output linearization, Eq. 6 is used to compute a net actuation torque from input current commands. The actuation torque is then used as an intermediate input to the black-box catheter system. The output angle and the intermediate torque input is then employed to perform linear system identification to identify this black-box linearized dynamics. The approximate planar pendulum model is chosen to put more emphasis on getting a conscise framework to analyze the system behavior instead of performing complex examinations of the out-of-plane nonlinearities to characterize the system. Thus, only axial coil is excited to apply planar actuation torque to system and side coils (Fig. 2b) are not used to generate out-of-plane input actuation torque.

A chirp signal with an amplitude of 100 mA and duration of 300 s that sweeps the frequency spectrum from 0.5 Hz to 8 Hz is used to excite the system. As the catheter design is axially symmetric, the system identification for the linearized model was only performed in one deflection-direction. Hence, the chirp signals were used only for axial coil excitation and thus yielded planar motions [19]. The fixed catheter length, L, used in pendulum model (Fig. 3b), yields reasonable approximation for the applied input chirp signals. The error between the actual length of the bending catheter (Fig. 3a) and the fixed catheter length (Fig. 3b) in the pendulum approximation is less than 3 mm at the maximum deflection angle (48 degrees).

The resulting motion of the catheter was measured using an external camera and catadioptric stereo tracking [28]. The final output of the catheter tracking is the location of the catheter tip and the tangent vector of the coil. The upper limit of the chirp sweep was chosen as 8 Hz in order to have sufficient number of deflection measurement samples per period (namely, 7 to 8 samples per period as recommended in the

TABLE I. THE FIT ERROR RESULTS OF THE ESTIMATED AND REDUCED ORDER MODELS TO TRAINING AND VALIDATION CHIRP SIGNALS. THE ERROR BETWEEN THE OBSERVED SIGNAL AND MODEL OUTPUT IS CALCULATED. FIT RESULTS ARE REPORTED BY CALCULATING THE ERROR SIGNAL ENERGY AS A PERCENTAGE OF OBSERVED SIGNAL ENERGY.

	Model Fit Error (%)	
Data (Duration [s])	15^{th} order	2^{nd} order
Training (300)	1.5109	3.2593
Validation 1 (360)	1.6524	4.6544
Validation 2 (300)	0.4682	1.4190

literature [29]) using the catadioptric stereo tracking system, which was operating at 60 Hz sampling rate. Frequencies beyond 8 Hz were also not excited to protect the catheter hardware.

The choice of the model structure to represent a system is driven by several factors such as coupling of plant and noise parametrization, estimation difficulty, and bias consideration. Autoregressive models with exogenous input (ARX) and output error (OE) models are the two common choices in the system identification literature [30], [31] as an initial selection for the model structure. Due to the limited knowledge of the black-box model *a priori* and high reliance on the data, an ARX model was selected as an initial structure in this study to characterize the system. As the ARX model family is linear in parameters, it provides an ease of computation for the optimal model selection order despite its highly restrictive parametrization, when compared to the OE family.

The optimal model order estimation using the net input actuation torque (where the magnetic torque is larger about an order of magnitude than the gravitational torque) and output angle data resulted in a 15^{th} order model. This optimal model is used to observe the system modes, which is then reduced to a 2^{nd} order approximate model using balanced truncation considering the Nyquist frequency of the camera, which is 30 Hz. The resulting system is given by the following transfer function:

$$H(s) = \frac{1.761e04s + 6344}{s^2 + 4.59s + 1.136}. \tag{7}$$

The bode plot of this system is superimposed on the estimated 15^{th} order model are given in Fig. 5. Based on the bode plot, the cut-off bandwidth of the system is estimated at around 1.3 Hz.

The resulting model is also examined using different chirp signals. The first planar validation signal sweeps the frequency spectrum from 1 Hz to 8 Hz and the second one sweeps 0.5 Hz to 4 Hz. For these chirp signals, the error signal between the observed signal and the model output is calculated. The error signal energy (by Parseval's theorem [32]) as a percentage of the observed signal energy for the estimated 15^{th} order and reduced 2^{nd} order models are given in Table I and model output for the validation signal with sweep from 1 Hz to 8 Hz is shown in Fig. 6. The reduced model can capture the overal signal characteristics across the frequency range and provides a reasonable trade off for model complexity.

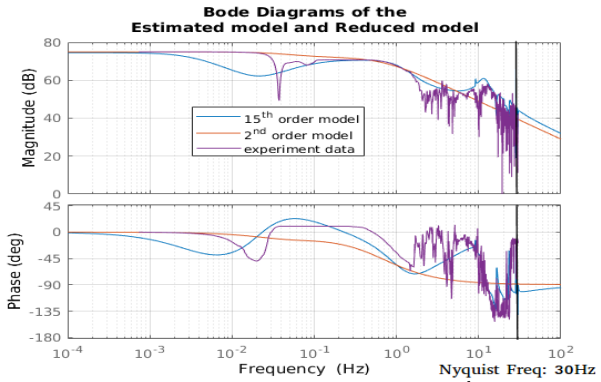

Fig. 5. Frequency response of the reduced 2^{nd} order transfer function superimposed on the the estimated 15^{th} order system. Also, shown are the experiment data and camera Nyquist frequency (drawn with a black line), which is used during the model reduction.

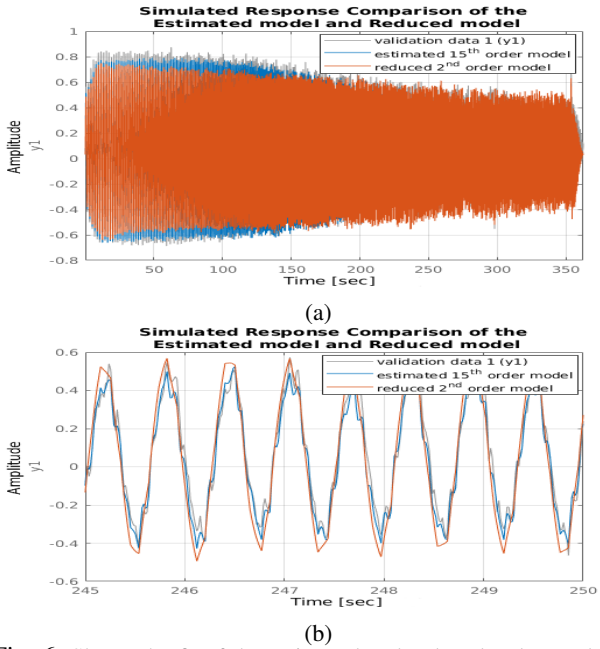

Fig. 6. Shows the fit of the estimated and reduced order models to validation chirp signal with sweep from 1 Hz to 8 Hz. (a) Original scale. (b) Magnified scale.

IV. VALIDATION EXPERIMENTS

A. Experimental Methods

A concise dynamic reponse analysis approach is presented in III. Inherent nonlinearity of the system is approximated and the frequency response of the system is calculated using in-plane motions. In this section, the validity of the results are examined using out-of-plane motions. Accordingly, the planar dynamic model is validated using $3D$ spatial deflection trajectories. Specifically, two distinct trajectories (lemniscate and circle) were used for validating the system behavior under the open-loop control. The trajectories of the catheter tip were obtained by projecting a $2D$ geometrical shape on to the catheter workspace [19]. These shapes are similar to the circumferential and linear ablation lesions employed in atrial fibrillation ablation [2]. Thus, they imitate realistic motions of the desired application and preferred to simply testing

catheter's response in various directions.

There are 200 points along a single period of each trajectory. With four repetitions, each trajectory has a total of 800 points. Each trajectory was commanded to the system with different pause times between the trajectory steps. Pause times are artificially introduced in between the trajectory steps in order to acquire multiple camera images at each step, which are averaged to reduce the noise in camera measurements. Experimental data was collected in multiple sessions, while each type of trajectory data was collected in a single session.

The current corresponding to each point on these trajectories was iteratively calculated using the Jacobian-based inverse kinematics method presented in [19]. The calculated currents were applied to actuate the catheter in the experiments. The deflection motions were recorded and tracked by the vision system.

B. Experiment Setup

The catheter prototype (Fig. 2) is embedded with one current-carrying coil set, which includes one 100-turn axial coil and two 30-turn orthogonal side coils. The coils are made of heavy insulated 38-gauge enameled copper wires (Adapt Industries, LLC, Salisbury, MD, USA). They are built over silicone rubber tubing (Part number: T2011, QOSINA, Edgewood, NY, USA). Please refer to [26] for further details about the catheter prototype.

The experiments were conducted in a $3\mathrm{T}$ clinical scanner (Skyra, Siemens Medical Solutions, Erlangen, Germany), as shown in Fig. 7a. The front view of the experiment setup is shown in Fig. 7b. The catheter prototype is mounted vertically inside an aquarium tank ($25.4\ \mathrm{cm} \times 25.4\ \mathrm{cm} \times 26.7\ \mathrm{cm}$) and immersed in a phantom filled with distilled water doped with a gadolinium-based contrast agent. The aquarium tank is centered along the central axis of the MRI scanner, but offset from the isocenter to accommodate a mirror which displays the catheter in side perspective. The mirror is needed because a camera cannot capture the side motions of the catheter well from outside the MRI scanner bore. The cables of the coils are connected to a transconductance amplifier controller which stays outside the MRI room. The controller box sets the coil currents using a microcontroller which communicates with a PC through a USB serial link. In this paper, the coil currents are limited to $100\ \mathrm{mA}$ [26], [33] , which was the maximum value allowed by the amplifier box. Before each experiment, an MRI image displaying the LEGO® bricks in a coronal slice was used for determining the alignment quality of the experiment setup with the direction of the constant magnetic field. The same experiment setup was used for the $2D$ planar deflection experiments.

C. Results

The deflection motions were recorded and tracked by the vision system. Fig. 8 shows a picture of the tracked catheter in the catadioptric image space. The final output of the catheter tracking is location of the catheter base, coil, and tip. The results also include the tangent vector of the coil. The validated catadioptric system provides high speed catheter tracking data that can be compared to the MRI tracking results as well as aid in frequency response modeling of the catheter as a part of future work. For further details please consult [28].

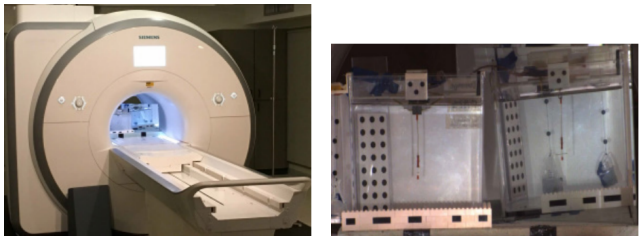

(a) (b)

Fig. 7. (a) Experiment setup inside a clinical MRI scanner. (b) Front view of the experiment setup. The catheter prototype is immersed in a phantom filled with distilled water doped with a gadolinium-based contrast agent. It is clamped vertically by a mechanism made from LEGO® bricks. The mirror next to the tank displays the actuated catheter in side perspective.

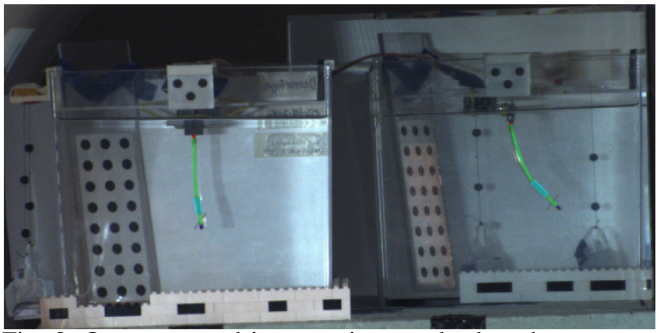

Fig. 8. One processed image using a color-based segmentation algorithm for the labeled markers located on the base, coil, and tip of the catheter. Green curves only simply connect the markers and are not intended to represent the whole body of the catheter.

Fig. 9a shows the vision-tracked positions of the labeled markers on the catheter (tip marker in blue, coil marker in green and base marker in yellow), which performed the given circular trajectory represented in red, with a $100\ \mathrm{ms}$ pause time between individual trajectory points.

The root-mean-square (RMS) error between observed trajectory captured by the vision system and the desired trajectory was computed to calculate the open-loop accuracy at different pause times.

As the implemented control is open-loop (which does not use any feedback from measurement of catheter position) and the catheter body is compliant, offsets between the given and observed trajectories are expected, shown in Fig. 9a[3].

The shapes of the trajectories were compared by ignoring position and orientation offsets. Specifically, the trajectories were allowed to be translated and rotated (but not scaled) until the RMS error between them is minimized, and the residual RMS error was used as the shape similarity measure.

The final results are reported in Fig. 9b shows the given

[3]A video attached to this manuscript demonstrates these catheter motions inside the MRI scanner.

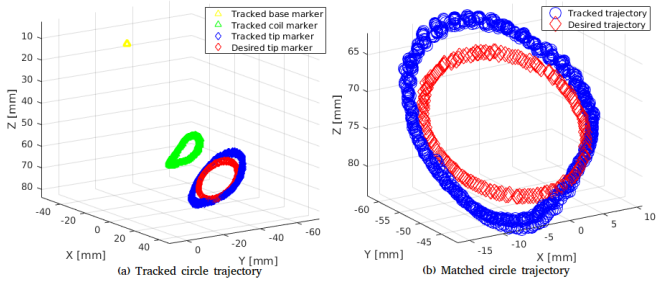

(a) Tracked circle trajectory (b) Matched circle trajectory

Fig. 9. Catheter trajectories tracked via camera-based vision system. Fig. 9a shows the tracked base, coil, and tip markers together with the desired marker trajectory. Fig. 9b shows the resulting tracked and desired trajectories after the rigid body transformation for alignment without scaling.

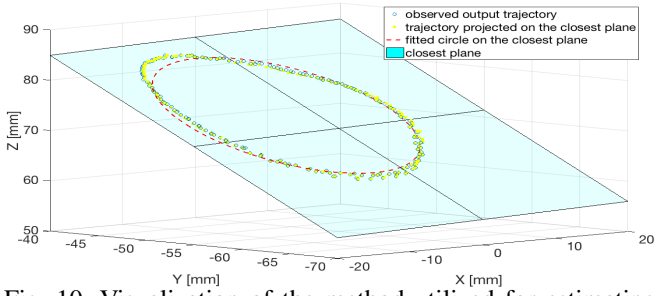

Fig. 10. Visualization of the method utilized for estimating the magnitude response for the catheter system based on observed output and input desired trajectories.

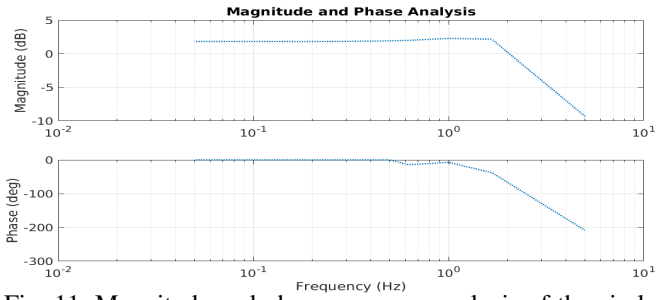

Fig. 11. Magnitude and phase response analysis of the circle trajectory

desired trajectory (red diamonds) and all the observed trajectories (blue markers) after a rigid body transformation alignments.

1) Evaluation of the Estimated Model: Dynamic response of the catheter system identified (Fig. 5) in Section III-B is evaluated. For this purpose, the magnitude and phase responses of the circular trajectory are estimated based on the desired input and observed output trajectories (Fig. 9b) at different pause times. Then, the computed magnitude and phase responses are compared with the dynamic response (Fig. 5) of the estimated model given in (7).

To compute the magnitude response, at each pause time, the closest plane to the observed $3D$ output trajectory was calculated using singular value decomposition [34]. The output trajectory was projected onto this plane. Then, a $2D$ circle on the plane frame was fitted to the projected trajectory points (Fig. 10). The same method was also applied to the desired input trajectory. The magnitude response is then calculated as the ratio of radii of the fitted circles to output and input trajectories:

$$Magnitude\,(\mathrm{dB}) = 20\log\frac{r_{output}}{r_{input}}, \tag{8}$$

where r_{output} and r_{input} are respectively radii of the fitted circles to output and input trajectories.

The phase response is estimated by computing the time delay between the input and output trajectories [35], where $3D$ cross correlation function is utilized to compute the time delay [32].

The maximum value of the cross correlation computation gives the lag difference, τ_{yx}, between the observed output and desired input trajectories. Time lag, Δt, between input and output is then given by multiplying the lag difference with the corresponding pause time, t_{pause}.

$$\Delta t = \tau_{yx} \cdot t_{pause}. \tag{9}$$

Subsequently, the phase shift between the input-output is given as:

$$Phase\,(\mathrm{deg}) = \frac{\Delta t}{T} \cdot 360^{\circ}, \tag{10}$$

where T is the period of trajectory with $T = N \times t_{pause}$, with $N = 200$ number of trajectory points per period and t_{pause} is the corresponding pause time in (9).

The estimated magnitude and phase responses are presented in Fig. 11, where frequency values are computed by taking the reciprocal of the trajectory period T from (10), $F = 1/T$. The magnitude response analysis shows that the cut-off (3 dB) frequency of the system is on the order of 1-2 Hz. Furthermore, phase response decreases significantly following system bandwidth. These observations match with the dynamic response analysis (Fig. 5) presented in Section III.

2) Evaluation of the Accuracy: The open-loop trajectory tracking accuracy of the catheter system at different pause times for both trajectories are given in Fig. 12 and Table II to show the tip tracking and coil tangent orientation results for circle and lemniscate trajectories at different pause times. The 60 Hz camera tracking system has a sampling period of approximately 16.7 ms. Thus, for pause times larger than the camera sampling period, it was possible to obtain individual tracking points per each input trajectory point. For pause times less than the camera sampling period, the tracking results were interpolated to match total number of input trajectory points.

The reported RMS error values for the pause times larger than 18 ms are consistent with the tracking results presented in [19] and are in the range of 2-4 mm. These errors are typical for open-loop control (and are expected to be eliminated by proper closed-loop control).

In the tracking error results presented in Fig. 13 and Table II, the tracking performance for both circle and lemniscate trajectories deteriorates significantly after 1-2 Hz. This points that the bandwidth of the system is this interval, which is consistent with frequency response analysis given in Section III.

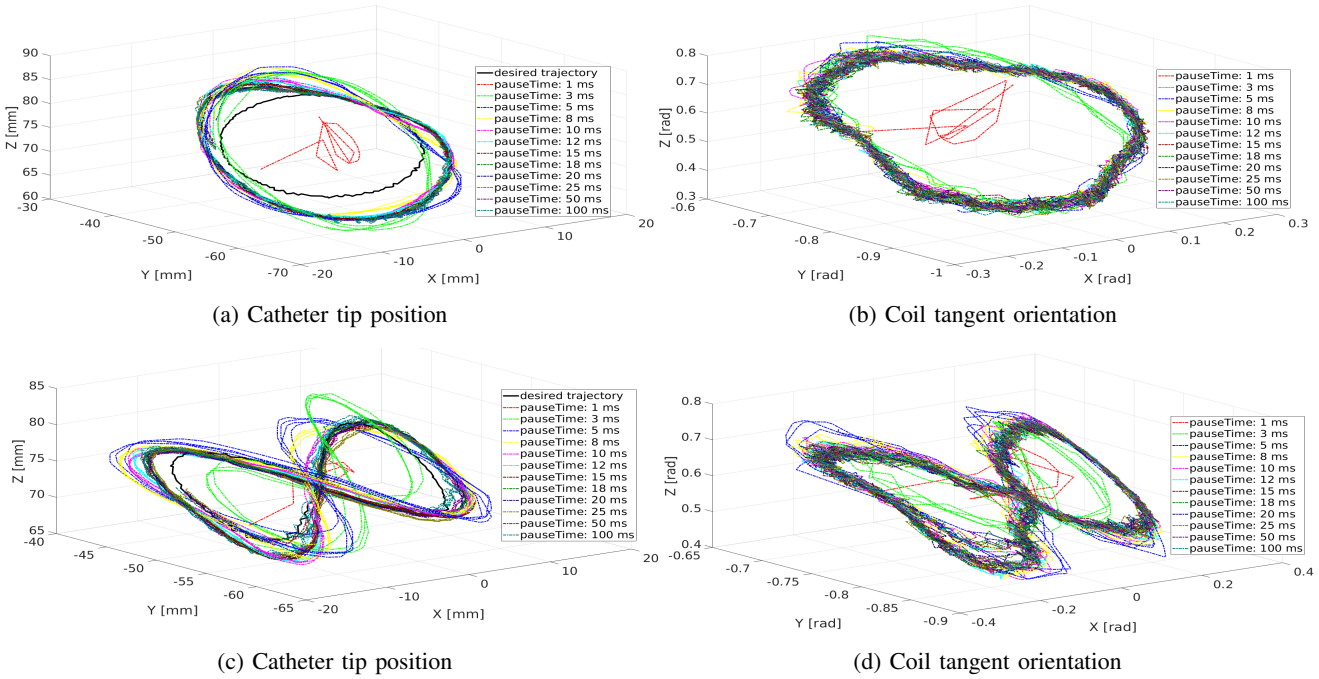

(a) Catheter tip position

(b) Coil tangent orientation

(c) Catheter tip position

(d) Coil tangent orientation

Fig. 12. Tracking results for circle and lemniscate trajectories at different pause time between trajectory points. Figs. 12a, 12c show tip location together with the desired trajectory. Figs. 12b, 12d show coil tangent orientation.

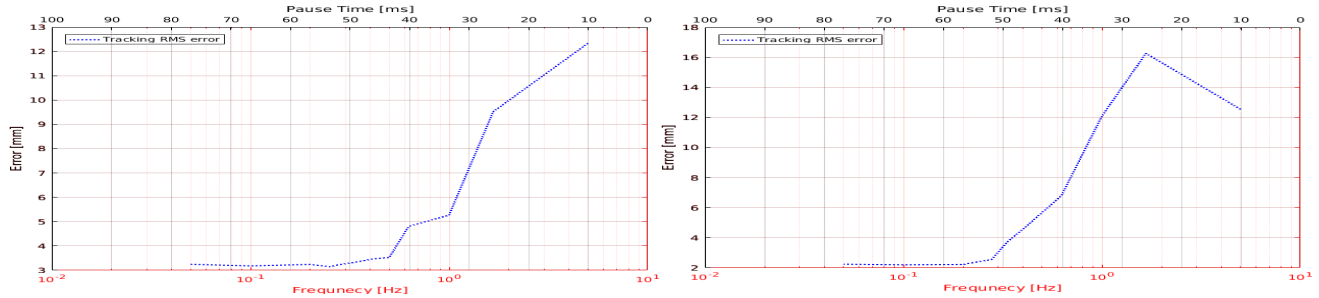

(a) Circle trajectory error

(b) Lemniscate trajectory error

Fig. 13. Tracking errors for circle and lemniscate trajectories at different pause times.

V. Discussion and Conclusion

In this paper, a dynamic response analysis of an MRI-guided magnetically-actuated steerable catheter is presented. In the presented approach, the system model is first approximately input-output linearized. Then, the remaining approximated linear dynamics is identified using black-box linear system identification techniques. The estimated system model is evaluated with Cartesian space trajectories under open-loop control of the catheter system in hardware experiments. The goal is to present a concise framework to perform system characterization, as apposed to modeling the complex system nonlinearites.

The optimal estimated model is reduced utilizing the balanced truncation method considering the Nyquest frequency of the camera system used to track the catheter. The reduced model shows satisfactory fit and the results demonstrated that the catheter has a bandwidth of approximately 1.3 Hz. The open-loop $3D$ tracking validation results presented in Section IV-C revealed a system bandwidth of 1-2 Hz, which is consistent with the system bandwidth of 1.3 Hz from the dynamic response analysis.

One source of discrepancy is that, the frequency response analysis Section III was performed with $2D$ planar trajectories, whereas the open-loop validation experiments in Section IV-C were performed with $3D$ trajectories. As this study is a first step to evaluate frequency response behavior of the proposed catheter system, a full system identification with open-loop and closed-loop $3D$ trajectories remains as

TABLE II. Shows the change in RMS catheter tip position at different pause times between trajectory samples for the lemniscate and circle trajectories.

Pause Time (ms)	1	3	5	8	10	12	15	18	20	25	50	100
Circle RMSE (mm)	12.33	9.51	5.26	4.80	3.52	3.46	3.32	3.22	3.14	3.24	3.17	3.24
Lemniscate RMSE (mm)	12.54	16.27	12.08	6.79	5.68	4.76	3.71	2.54	2.45	2.22	2.19	2.24

a future work.

Additionally, this analysis only reveals the system behavior for free-space trajectories as the goal is to pave the way for free-space closed-loop control. As the catheter ablation procedure is performed in contact with the tissue (Fig. 1a), the free-space closed loop control will be followed by the in-contact dynamic response analysis and subsequently catheter surface motion control. Thus, the surface-motion dynamic response analysis will be addressed in the subsequent research and is outside the scope of this study.

As the catheter moves relatively slow, the impact of the surrounding medium was not considered. The unmodeled system dynamics remain as the other sources of error.

This analysis together with [19] paves the way for effective and accurate control of the robotic catheter in a closed-loop control system with feedback information from real-time MRI-guidance. The open-loop accuracy level makes it reasonable to expect that a closed-loop control system can achieve the desired $1\ \mathrm{mm}$ accuracy level.

REFERENCES

[1] *What Is Catheter Ablation?*, National Heart Lung and Blood Institute, http://www.nhlbi.nih.gov/health/health-topics/topics/ablation/.

[2] J. Dewire and H. Calkins, "State-of-the-art and emerging technologies for atrial fibrillation ablation," *Nat. Rev. Cardiol.*, vol. 7, pp. 129–138, 2010.

[3] *Niobe ES Magnetic Navigation System*, Stereotaxis, http://www.stereotaxis.com/niobe.html.

[4] *Sensei X Robotic Catheter System*, Hansen Medical, http://www.hansenmedical.com/.

[5] T. Liu and M. C. Cavusoglu, "Three dimensional modeling of an MRI actuated steerable catheter system," in *Proc. IEEE Int. Conf. Robot. Autom.*, May 2014, pp. 4393–4398.

[6] S. Nazarian, A. Kolandaivelu, M. M. Zviman, G. R. Meininger, R. Kato, R. C. Susil, A. Roguin, T. L. Dickfeld, H. Ashikaga, H. Calkins, R. D. Berger, D. A. Bluemke, A. C. Lardo, and H. R. Halperin, "Feasibility of Real-Time Magnetic Resonance Imaging for Catheter Guidance in Electrophysiology Studies," *Circulation*, vol. 118, no. 3, pp. 223–229, July 2008.

[7] S. Schalla, M. Saeed, C. B. Higgins, A. Martin, O. Weber, and P. Moore, "Magnetic resonance–guided cardiac catheterization in a swine model of atrial septal defect," *Circulation*, vol. 108, no. 15, pp. 1865–1870, 2003.

[8] T. P. L. Roberts, W. V. Hassenzahl, S. W. Hetts, and R. L. Arenson, "Remote control of catheter tip deflection: An opportunity for interventional MRI," *Magn. Reson. Med.*, vol. 48, no. 6, pp. 1091–1095, 2002.

[9] F. Settecase, M. S. Sussman, M. W. Wilson, S. Hetts, R. L. Arenson, V. Malba, A. F. Bernhardt, W. Kucharczyk, and T. P. L. Roberts, "Magnetically-assisted remote control (MARC) steering of endovascular catheters for interventional MRI: a model for deflection and design implications," *Med. Phys.*, vol. 34, no. 8, pp. 3135–3142, August 2007.

[10] V. Lalande, F. P. Gosselin, and S. Martel, "Catheter steering using a magnetic resonance imaging system," in *Conf. Proc. IEEE Eng. Med. Biol. Soc.*, Aug. 31 - Sep. 4 2010.

[11] I. Tunay, "Modeling magnetic catheters in external fields," in *Conf. Proc. IEEE Eng. Med. Biol. Soc.*, San Francisco, CA, USA, September 1-5, 2004, pp. 2006–2009.

[12] R. S. Sincic, C. J. Caton, P. Lillaney, S. Goodfriend, J. Ni, A. J. Martin, A. D. Losey, N. Shah, E. J. Yee, L. Evans, V. Malba, A. F. Bernhardt, F. Settecase, D. L. Cooke, M. Saeed, M. W. Wilson, and S. W. Hetts, "System architecture for a magnetically guided endovascular microcatheter," *Biomed. Microdevices*, vol. 16, no. 1, pp. 97–106, 2014.

[13] F. Ullrich, S. Schuerle, R. Pieters, A. Dishy, S. Michels, and B. J. Nelson, "Automated capsulorhexis based on a hybrid magnetic-mechanical actuation system," in *Proc. IEEE Int. Conf. Robot. Autom.*, May 2014, pp. 4387–4392.

[14] M. N. Faddis, W. Blume, J. Finney, A. Hall, J. Rauch, J. Sell, K. T. Bae, M. Talcott, and B. Lindsay, "Novel, magnetically guided catheter for endocardial mapping and radiofrequency catheter ablation," *Circulation*, vol. 106, no. 23, pp. 2980–2985, 2002.

[15] N. Gudino, J. A. Heilman, J. J. Derakhshan, J. L. Sunshine, J. L. Duerk, and M. A. Griswold, "Control of intravascular catheters using an array of active steering coils," *Med. Phys.*, vol. 38, no. 7, pp. 4215–4224, 2011.

[16] T. Liu, N. Lombard Poirot, D. Franson, N. Seiberlich, M. Griswold, and M. Cavusoglu, "Modeling and validation of the three dimensional deflection of an mri-compatible magnetically-actuated steerable catheter," *IEEE Trans. Biomed. Eng.*, vol. PP, no. 99, pp. 1–1, 2016.

[17] Y. Fu, H. Liu, W. Huang, S. Wang, and Z. Liang, "Steerable catheters in minimally invasive vascular surgery," *Int. J. Med. Robot. Comp.*, vol. 5, no. 4, pp. 381–391, 2009.

[18] K. Ikuta, H. Ichikawa, K. Suzuki, and D. Yajima, "Multi-degree of freedom hydraulic pressure driven safety active catheter," in *Proc. IEEE Int. Conf. Robot. Autom.*, May 2006, pp. 4161–4166.

[19] T. Liu, R. Jackson, D. Franson, N. L. Poirot, R. K. Criss, N. Siberlich, M. A. Griswold, and M. C. Cavusoglu, "Iterative jacobian-based inverse kinemarics and open-loop control of an mri-guided magneticalyl-actuated steerable catheter system," *IEEE/ASME Trans. Mechatronics*, vol. Accepted, 2017.

[20] J. J. More, *The Levenberg-Marquardt algorithm: Implementation and theory*. Berlin, Heidelberg: Springer Berlin Heidelberg, 1978, pp. 105–116.

[21] S. R. Buss, "Introduction to inverse kinematics with jacobian transpose, pseudoinverse and damped least squares methods," Tech. Rep., 2004.

[22] S. R. Buss and J.-S. Kim, "Selectively damped least squares for inverse kinematics," *J. Grap. T.*, pp. 37–49, 2004.

[23] A. D. Marchese, R. Tedrake, and D. Rus, "Dynamics and trajectory optimization for a soft spatial fluidic elastomer manipulator," *Int. J. Rob. Res.*, vol. 35, no. 8, pp. 1000–1019, July 2016. [Online]. Available: http://dx.doi.org/10.1177/0278364915587926

[24] R. S. Penning, J. Jung, N. J. Ferrier, and M. R. Zinn, "An evaluation of closed-loop control options for continuum manipulators," in *2012 IEEE International Conference on Robotics and Automation*, May 2012, pp. 5392–5397.

[25] M. Gilbertson, D. Beekman, B. Mohanty, S. Hashemi, S. Lee, J. Van De Ven, and T. Kowalewski, *Force analysis and modelling of soft actuators for catheter robots*. American Society of Mechanical Engineers, 2016, vol. 2, p. 78DUMMY.

[26] T. Liu, N. L. Poirot, T. Greigarn, and M. Cavusoglu, "Design of an mri-guided magnetically-actuated steerable catheter," *ASME J. Med. Devices*, 2017.

[27] R. M. Murray, Z. Li, and S. S. Sastry, *A Mathematical Introduction to Robotic Manipulation*, 1st ed. Boca Raton, FL: CRC Press, 1994.

[28] R. C. Jackson, T. Liu, and M. Cavusoglu, "Catadioptric stereo tracking for three dimensional shape measurement of mri guided catheters," in *Proc. IEEE Int. Conf. Robot. Autom.*, May 2016.

[29] G. F. Franklin, M. L. Workman, and D. Powell, *Digital Control of Dynamic Systems*, 3rd ed. Boston, MA, USA: Addison-Wesley Longman Publishing Co., Inc., 1997.

[30] L. Ljung, Ed., *System Identification (2Nd Ed.): Theory for the User*. Upper Saddle River, NJ, USA: Prentice Hall PTR, 1999.

[31] T. Söderström and P. Stoica, Eds., *System Identification*. Upper Saddle River, NJ, USA: Prentice-Hall, Inc., 1988.

[32] A. V. Oppenheim and R. W. Schafer, *Discrete-Time Signal Processing*, 3rd ed. Upper Saddle River, NJ, USA: Prentice Hall Press, 2009.

[33] S. Hetts, M. Saeed, A. Martin, L. Evans, A. Bernhardt, V. Malba, F. Settecase, L. Do, E. Yee, A. Losey, R. Sincic, P. Lillaney, S. Roy, R. Arenson, and M. Wilson, "Endovascular catheter for magnetic navigation under mr imaging guidance: Evaluation of safety in vivo at 1.5t," *American Journal of Neuroradiology*, vol. 34, no. 11, pp. 2083–2091, 2013. [Online]. Available: http://www.ajnr.org/content/34/11/2083

[34] K. S. Arun, T. S. Huang, and S. D. Blostein, "Least-squares fitting of two 3-d point sets," *IEEE Trans. Pattern Anal. Mach. Intell.*, vol. 9, no. 5, pp. 698–700, May 1987.

[35] P. Stoica and R. L. Moses, *Spectral Analysis of Signals*. Upper Saddle River, NJ: Prentice Hall, 2005.